Acta Cryst. (1968). B**24**, 1004

The Crystal Structure of ε-$Mg_{23}Al_{30}$*

BY STEN SAMSON AND E. KENT GORDON

Gates and Crellin Laboratories of Chemistry, California Institute of Technology, Pasadena, California 91109, *U.S.A.*

(*Received* 5 *June* 1967 *and in revised form* 1 *November* 1967)

A determination of the crystal structure of the ε phase in the magnesium–aluminum system has been carried out, and the structure has been refined by three-dimensional, least-squares techniques. The final agreement index R is 0·021 for 1469 reflections. The crystals are rhombohedral, space group $R\bar{3}$ with $a_0 = 10{\cdot}3625 \pm 0{\cdot}0003$ Å and $\alpha = 76°\,27{\cdot}7' \pm 0{\cdot}2'$; the corresponding hexagonal cell has the dimensions $a_0 = 12{\cdot}8254 \pm 0{\cdot}0003$ Å and $c_0 = 21{\cdot}7478 \pm 0{\cdot}0009$ Å. There are 53 atoms in the unit rhombohedron, distributed among 11 crystallographically different positions. The composition as deduced from the observed coordination numbers corresponds to $Mg_{23}Al_{30}$, but chemical analyses and measured densities of single-phase samples point to the formula $Mg_{22}Al_{31}$, indicating a small degree of substitutional disorder. A large portion of the structure consists of an infinite, three-dimensional framework of Friauf polyhedra that are penetrated by icosahedra, a feature that is observed in all intermediate magnesium–aluminum phases. Although this structure is similar to that of the R(Mo–Co–Cr) phase, there are significant differences in the structural parameters and hence also in the coordination polyhedra; it does not seem justified to call ε and R fully isostructural.

Introduction

Three intermediate phases have been shown with certainty to exist in the magnesium–aluminum system; the β phase of approximate composition Mg_2Al_3 (Perlitz, 1944, 1946; Samson, 1965), the ε phase of composition near Mg_4Al_5 (Kurnakov & Mikheeva, 1938; Clark & Rhines, 1957), and the γ phase, which has a range of homogeneity extending approximately from Mg_4Al_5 to $Mg_{17}Al_{12}$ at about 450 °C. The latter formula corresponds exactly to an ordered atomic arrangement of the $A12$ type (α-manganese) with 34 magnesium atoms and 24 aluminum atoms per unit cube of edge $a_0 = 10{\cdot}6$ Å (Laves, Löhberg & Rahlfs, 1934). Accordingly, as many as about nine of the magnesium atoms in the unit cube of the ordered structure ($Mg_{17}Al_{12}$) can be replaced by aluminum without a basic change in the atomic arrangement. This aluminum-rich phase can be retained at room temperature only after rapid cooling from about 450 °C.†

The ε phase is formed after subsequent annealing of such an aluminum-rich γ-phase sample at or below about 370 °C; γ-phase samples rich in magnesium (up to $Mg_{17}Al_{12}$) are stable, even after prolonged annealing at any temperature below the melting point.

The phase change γ to ε is not an allotropic transformation. It is believed (Eickhoff & Vosskühler, 1953) that the aluminum-rich γ phase splits up into a peritectoid mixture of a magnesium-rich γ phase and the β phase, and that this mixture reacts to form the ε phase at or below 370 °C.

Powder X-ray photographs of the ε phase are extremely complex and single crystals are hard to obtain; the nature of this phase remained unknown for about 30 years.

Experimental

Composition and density

Powder X-ray techniques employing crystal-monochromatized Cu $K\alpha$ radiation (Guinier–Hägg camera) were used for the phase investigation; the suitability of such a camera for this purpose was demonstrated recently (Samson, 1967*a*). Since X-ray diffraction data do not suffice for determining with certainty the distribution of magnesium and aluminum atoms over the occupied atomic positions, the composition of the ε phase was established by chemical analyses of single-phase samples.

Powder-diffraction photographs of several two-phase samples of the kind β+ε and ε+γ indicated that the composition Mg_4Al_5 reported by Kurnakov & Mikheeva (1938) and Clark & Rhines (1957) was at least approximately correct. About 50 g of an alloy of this composition was prepared by melting together pieces of the metals of 99·9% purity in an aluminum-oxide crucible under dried argon gas at atmospheric pressure. The melt was thoroughly stirred with an aluminum-oxide rod and then cast into a watercooled, cylindrical copper mold. Part of the ingot was annealed at 340 °C for 144 hours and then quenched in ice water. The well-resolved, sharp and clear powder pattern obtained with the use of this sample (sample no. 1) indicated the presence of only one phase, the ε phase.

A second ingot of the same nominal composition, annealed for 4600 hours at 380 to 395 °C, contained

* Contribution No. 3530 from Gates and Crellin Laboratories of Chemistry. This work was supported by Grant No. GP-4237 from the National Science Foundation.

† One of us (S.S.) has refined the structure of a γ-phase crystal of composition near $Mg_{13}Al_{16}$ quenched from 450 °C (the agreement index R was 0·06) and found that the atomic arrangement did not deviate from that of the $A12$ type. A crystal of composition near $Mg_{17}Al_{12}$ is being investigated.

β and γ but not ε, and a third ingot (same composition) annealed for 3900 hours at 360 to 370 °C represented, again, the single ε phase and contained crystals that were suitable for the X-ray diffraction work (sample No. 2).

The density of each alloy was determined by the flotation method (tetrabromoethane and benzene), and each single-phase sample was chemically analyzed at a commercial laboratory. The results were as follows:

Sample No. 1

Mg 39·24%, Al 60·64%; *i.e.* $Mg_{3\cdot59}Al_5$
Mg 39·35%, Al 60·58%; *i.e.* $Mg_{3\cdot61}Al_5$ } $\varrho_m =$ 2·203 (3) g.cm^{-3}.

Sample no. 2

Mg 39·45%, Al 60·53%; *i.e.* $Mg_{3\cdot63}Al_5$
Mg 39·35%, Al 60·53%; *i.e.* $Mg_{3\cdot61}Al_5$ } $\varrho_m =$ 2·203 (3) g.cm^{-3}.

A γ-phase crystal (cubic), isolated from an alloy of composition Mg_4Al_5 quenched from about 420 °C ($a_0 = 10{\cdot}442 \pm 0{\cdot}002$ Å), was found by the flotation method to have a density of $\varrho_m = 2{\cdot}20 \pm 0{\cdot}02$ g.cm^{-3}. Hence, the packing efficiency of the atoms is very nearly the same for ε and γ.

Unit cell and space group

Irregular pieces isolated from the fractured ε phase (sample No. 2) were found with the use of a Buerger precession camera to be rhombohedral. Rotation and Weissenberg photographs confirmed this finding, and there were no systematic extinctions. The Laue symmetry is $\bar{3}$, and hence, the probable space group is either $R3$ or $R\bar{3}$.

The unit-cell parameters were determined from a photograph taken in a locally built precision Weissenberg camera of 10 cm diameter with the film placed in the asymmetric position. The crystal was rotated around the hexagonal a axis. Nickel-filtered Cu $K\alpha$ radiation was used ($\lambda\alpha_1 = 1{\cdot}54051$ Å, $\lambda\alpha_2 = 1{\cdot}54433$ Å). A least-squares refinement based on 28 high-angle reflections that were assigned hexagonal indices gave $a_0 = 12{\cdot}8254 \pm 0{\cdot}0003$ Å and $c_0 = 21{\cdot}7478 \pm 0{\cdot}0009$ Å. The corresponding rhombohedral cell (obverse relationship) has the parameters $a_0 = 10{\cdot}3625 \pm 0{\cdot}0003$ Å and $\alpha = 76°\,27{\cdot}7' \pm 0{\cdot}2'$.

Intensity data

Several irregular pieces, believed to be single-crystal fragments of the ε phase, were ground to spheres according to Bond (1951) and investigated for quality with the use of photographic techniques. One such sphere of 0·055 mm radius, aligned with the hexagonal c axis parallel to the φ axis, was used for the collection of intensity data on a Datex-automated, General Electric XRD-5 Diffractometer equipped with the one-quarter circle goniostat, a copper-target X-ray tube with nickel filter, a NaI(Tl) scintillation counter prepared according to Samson (1966), and Nuclear–Chicago counter circuitry with a pulse-height analyzer. Since the pulse amplitude remained constant over the entire intensity range (no gain shift), a window of 90% transmission was used. The diffractometer was accurately aligned according to the description given by Samson & Schuelke (1967). The high voltage (constant potential) for the X-ray tube was kept constant to within ± 5 volts with the use of an inductively coupled, series-tube regulator that was built locally according to Pepinsky & Jarmotz (1948). The linearity of the counter is easily and reliably tested according to Short (1960).

The $2\theta{:}\theta$-scan method was used throughout with a scanning speed of 1 degree per minute, and the background was determined on either side of each peak from the number of counts accumulated in 100 seconds. The doublets $\alpha_1\alpha_2$ were always measured together in a single scan. About 150 reflections are extremely weak and the value used is the average of several measurements.

There were reasons to suspect that, during some measurements, a multiple reflection (Renninger, 1937) was superimposed on a Bragg reflection, thereby causing the intensity to come out too high. Several errors of this kind were indeed found and remedied as described in the next section.

Spherical absorption-correction factors ($\mu R = 0{\cdot}54$) and Lorentz and polarization factors were applied to the measured intensities and their standard deviations.

Avoidance of some systematic Renninger interactions

It is well known that a Renninger reflection $h_1k_1l_1$ can occur if the reciprocal-lattice point $h_1k_1l_1$ lies upon the sphere of reflection simultaneously with a reciprocal-lattice point $h_2k_2l_2$ and when a third reflection $h_3k_3l_3$ exists that satisfies the conditions $h_1 = h_2 + h_3$, $k_1 = k_2 + k_3$, $l_1 = l_2 + l_3$; both $h_2k_2l_2$ and $h_3k_3l_3$ must be strong reflections.

Since our crystal was aligned with the c axis parallel to the φ axis, the reciprocal-lattice vector $\bar{\mathbf{v}}_1$, passing through $h_1k_1l_1$, forms the angle $90 - \chi_{h_1k_1l_1}$ with the vector $\bar{\mathbf{v}}_2$, passing through $00l_2$. When the two reciprocal-lattice points $h_1k_1l_1$ and $00l_2$ lie upon the sphere of reflection, then the primary X-ray beam forms the angle $90 - \theta_{h_1k_1l_1}$ with $\bar{\mathbf{v}}_1$ and $90 - \theta_{00l_2}$ with $\bar{\mathbf{v}}_2$. The vectors $\bar{\mathbf{v}}_1, \bar{\mathbf{v}}_2$ and the center line of the primary X-ray beam then give rise to a right-angled, spherical triangle that has the sides $a = 90 - \chi_{h_1k_1l_1}$, $b = 90 - \theta_{00l_2}$, $c = 90 - \theta_{h_1k_1l_1}$, and $B = 90°$, since the χ plane is perpendicular to the plane defined by the primary and reflected ($h_1k_1l_1$) X-ray beam. Napier's rule then gives

$$\sin \theta_{00l_2} = \sin \theta_{h_1k_1l_1} \cdot \sin \chi_{h_1k_1l_1} .$$

Since $\sin \theta_{00l_2} = 0{\cdot}5\lambda c^* l_2$, and $\sin \theta_{h_1k_1l_1} \cdot \sin \chi_{h_1k_1l_1} = 0{\cdot}5\lambda c^* l_1$, the only necessary condition for $h_1k_1l_1$ to lie upon the sphere simultaneously with $00l_2$ is that $l_1 = l_2$. Consequently, any strong $00l$ reflection ($00l_2$) may interact with any strong $hk0$ reflection (h_3k_30) to pro-

duce the Renninger reflection hkl ($h_1k_1l_1 \equiv 00l_2 + h_3k_30 = h_3k_3l_2$).

Since crystals of complex intermetallic compounds very often give strong reflections of the type $h00$, *etc.* and $hk0$, *etc.*, but very weak reflections of the type hkl ($l \neq 0$), it seems advisable to avoid using a principal axis as rotation axis (parallel φ); see also Burbank (1965).

In the present case the reflections 009 and 0,0,15 ($h_2k_2l_2$) are very strong, as are the reflections 360, 390, 410, 710, and 820 ($h_3k_3l_3$). The twenty $h_1k_1l_1$ reflections (369, 3,6,15, 399, 3,9,15, ... *etc.*) were suspected to be overlapped completely or partially (depending upon the accuracy of crystal alignment and instrument settings) by Renninger reflections. Each of these was remeasured with the crystal tilted by about 5 degrees with respect to the φ axis. Eight of the new measurements resulted in significantly decreased F_{obs} values as is shown in Table 1. For the remaining twelve $h_1k_1l_1$ reflections the Renninger interaction was too weak to be detected, and the Bragg reflections on which they were superimposed were relatively strong.

Table 1. *The effect of Renninger interactions on some measured structure factors*

The F_{obs} values shown in column 2 were obtained with the c axis parallel to the φ axis, and those in column 3 with the c axis tilted by 5° with respect to the φ axis. The higher values (column 2) result from overlap with Renninger reflections.

h_1	k_1	l_1	F_{obs} c axis ‖ φ	F_{obs} c axis offset	σF_{obs}
3	6	9	197	93	19
3	6	$\bar{15}$	414	364	11
4	1	9	523	77	22
4	1	$\bar{9}$	695	333	9
4	1	15	1265	1186	10
4	1	$\bar{15}$	1450	1294	15
7	1	$\bar{15}$	393	281	13
8	2	9	185	76	23

Derivation of the trial structure

Previous crystal-structure studies of γ-$Mg_{17}Al_{12}$ (Laves *et al.*, 1934), $Mg_3Cr_2Al_{18}$, β-Mg_2Al_3 (Samson, 1958, 1965), and $Mg_{32}(Zn,Al)_{49}$ (Bergman, Waugh & Pauling, 1957), as well as knowledge of the reaction γ-$Mg_{<17}Al_{>12}$ + β-Mg_2Al_3 → ε-$Mg_{\sim 4}Al_{\sim 5}$, led to the hypothesis that the dominant coordination shells in the ε phase are Friauf polyhedra and icosahedra. A structurally very attractive Friauf-polyhedra framework was quickly fitted into the rhombohedral unit cell of assumed space group $R\bar{3}$, and there was very limited reasonable latitude to fill the space if the fundamental structural principles outlined recently (Samson, 1967*a*,*b*) were assumed to be applicable here. The Friauf-polyhedra framework comprises all but the two crystallographically different atoms Mg(1) and Mg(2) located on the threefold axis of the rhombohedron.

Assignment of magnesium and aluminum to the various point sets was made to fit the assumption that the large atoms (magnesium) have a ligancy larger than twelve and the small atoms (aluminum) a ligancy equal to or smaller than twelve. This distribution of atoms, which corresponds to the one given in Table 2, accounts for one formula unit of $Mg_{23}Al_{30}$ per rhombohedral unit cell as compared with $Mg_{22}Al_{31}$, which corresponds to the chemical analyses (see composition and density); the calculated density is $\varrho_c = 2{\cdot}201$ g.cm^{-3}.

Except for the estimated approximate positional parameters for Mg(2) and Al(11) (Table 2), the trial structure is nearly identical with the refined model.

Refinement of the structure

With the atoms placed in the 11 different positions given in Table 2, a very promising agreement between observed and calculated structure factors was obtained.

The 26 positional parameters, the 11 isotropic temperature factors, and the scale factor were refined by full-matrix (38 × 38), least-squares calculations on the Institute's IBM 7040–7094 crystallographic computing system CRYRM (Duchamp, 1964). Space group $R\bar{3}$ is treated in this program with hexagonal parameters and indices, and these are given in Tables 2 and 4, respectively. The scattering factors listed in Table 3.3.1A of *International Tables for X-ray Crystallography* (1962) were employed. The weighting scheme was that

Table 2. *The positional parameters of* ε-$Mg_{23}Al_{30}$

The parameters (× 10^5) refer to the hexagonal unit cell. Column 2 gives the identification symbols used for the corresponding point sets in the R phase. Column 3 refers to the notation used in *International Tables for X-Ray Crystallography* (1952), p. 252.

	R-phase designation	Point set	X	Y	Z
Mg(1)	$A1$	3(b)	0	0	½
Mg(2)	$A2$	6(c)	0	0	33926 (4)
Mg(3)	$D1$	6(c)	0	0	07712 (3)
Mg(4)	$D2$	18(f)	26287 (4)	04320 (4)	12466 (2)
Mg(5)	$C1$	18(f)	43644 (4)	07282 (4)	01534 (2)
Mg(6)	$B2$	18(f)	17556 (4)	39857 (4)	20706 (2)
Al(7)	$A3$	18(f)	08890 (4)	23632 (4)	00171 (2)
Al(8)	$A4$	18(f)	22991 (4)	26550 (4)	10453 (2)
Al(9)	$A5$	18(f)	11604 (4)	13180 (4)	20143 (2)
Al(10)	$A6$	18(f)	21908 (4)	03171 (4)	27175 (2)
Al(11)	$B1$	18(f)	18443 (4)	44428 (4)	07118 (2)

Table 3. *Anisotropic* ($\times 10^3$) *and isotropic* (*column* 8) *temperature factors for* ε-$Mg_{23}Al_{30}$

	β_{11}	β_{22}	β_{33}	β_{12}	β_{13}	β_{23}	B (iso)
Mg(1)	2·89 (6)	β_{11}	1·56 (3)	β_{11}	0	0	1·97 (3)
Mg(2)	2·69 (4)	β_{11}	1·31 (2)	β_{11}	0	0	1·71 (2)
Mg(3)	2·96 (4)	β_{11}	0·68 (1)	β_{11}	0	0	1·39 (2)
Mg(4)	3·35 (4)	3·07 (4)	0·69 (1)	3·35 (6)	−0·10 (3)	−0·05 (3)	1·44 (1)
Mg(5)	3·35 (4)	2·76 (4)	0·72 (1)	3·39 (6)	−0·27 (3)	−0·36 (3)	1·39 (1)
Mg(6)	2·61 (4)	3·16 (4)	0·74 (1)	2·09 (6)	−0·06 (3)	0·06 (3)	1·47 (1)
Al(7)	2·27 (3)	2·45 (3)	0·66 (1)	2·33 (5)	−0·23 (2)	0·11 (2)	1·17 (1)
Al(8)	2·74 (3)	2·76 (3)	0·61 (1)	2·99 (5)	−0·02 (2)	0·07 (2)	1·23 (1)
Al(9)	2·48 (3)	2·35 (3)	0·66 (1)	2·41 (5)	0·09 (2)	0·10 (2)	1·19 (1)
Al(10)	2·42 (3)	2·74 (3)	0·76 (1)	2·89 (5)	−0·42 (2)	−0·25 (2)	1·29 (1)
Al(11)	3·10 (3)	2·66 (3)	0·72 (1)	3·13 (5)	0·39 (2)	0·03 (2)	1·35 (1)

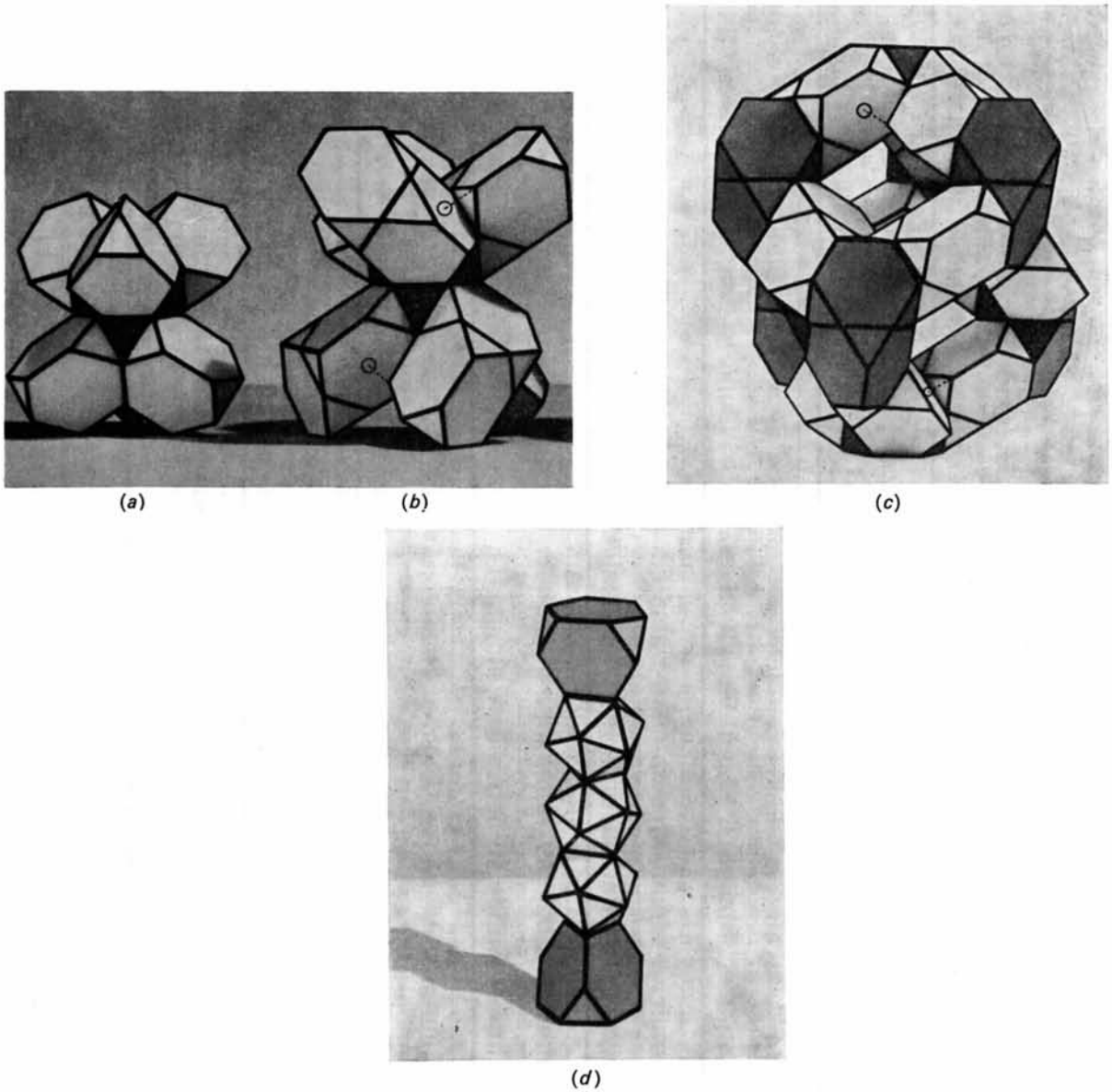

Fig. 1. (*a*) The arrangement of the Friauf polyhedra *F*2 (light) around *F*1 (dark). (*b*) A complex of 14 Friauf polyhedra. The origin of the rhombohedron coincides with the center of this complex. Two hybrid vertices discussed in the text are marked out. (*c*) The arrangement of Friauf polyhedra along the edges of the rhombohedral unit cell. (*d*) The arrangement of polyhedra along the threefold axis of the rhombohedron as it occurs in the *R* phase. In ε-$Mg_{23}Al_{30}$ the central icosahedron is replaced by the *L*14 shell, shown in Fig. 3, and each of the two other by an *L*13 shell, as shown in Fig. 2.

Table 4. *Observed and calculated structure factors*

The indices refer to the hexagonal unit cell. Each group of four columns contains, from left to right, indices l, observed structure factors, standard deviations $\sigma\,|F|$, and calculated structure factors. Here $\sigma\,|F| = [F^2 + \sigma(F^2)]^{1/2} - F$.

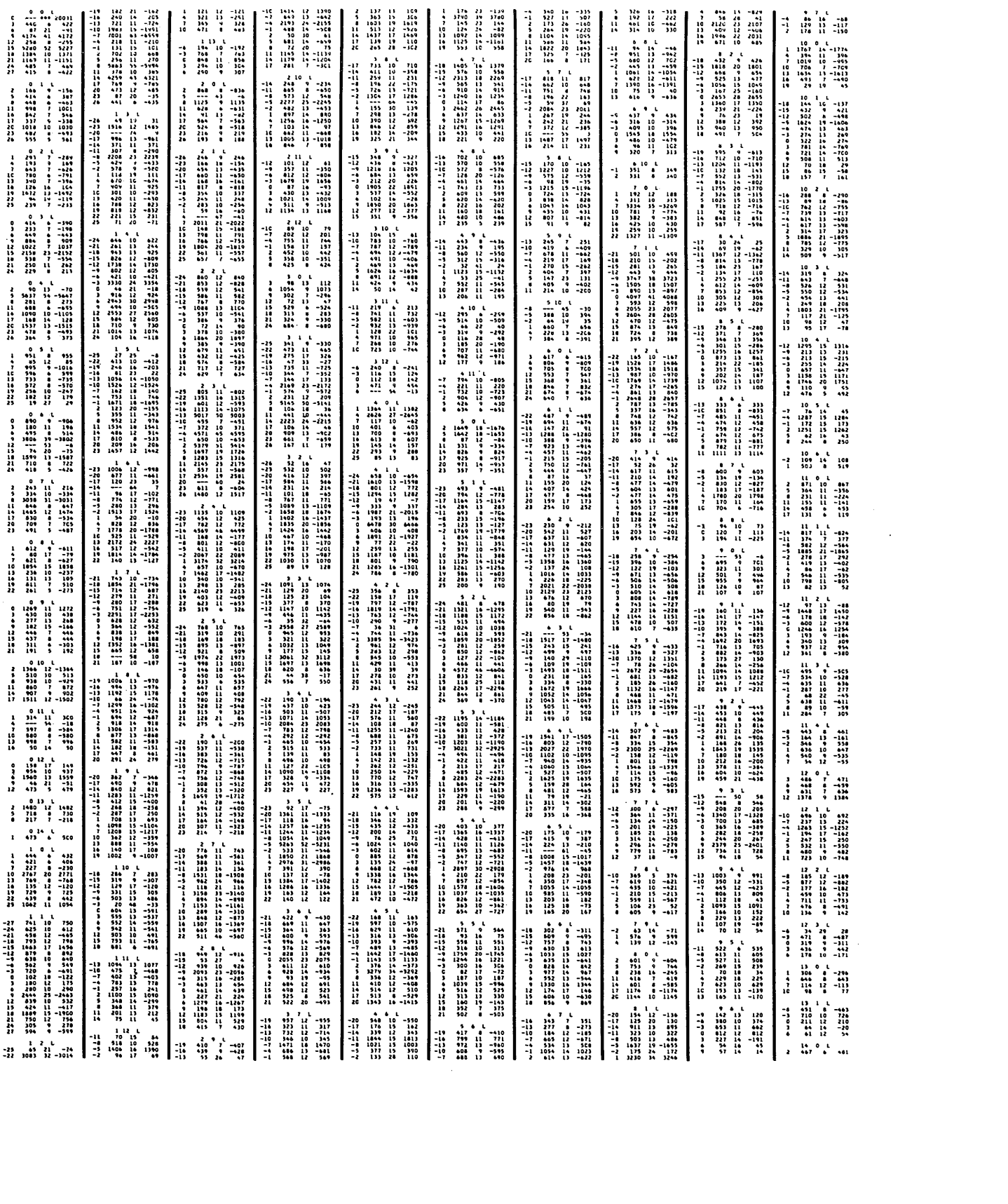

described by Peterson & Levy (1957), modified so as to apply to F^2 rather than to $F-\sigma(F^2)=2F\sigma(F)$– since the quantity minimized was $\Sigma\,\omega(F_o^2-F_c^2)^2$, where $\omega=[\sigma(F^2)]^{-2}$. Full shifts were used throughout.

The R index $\Sigma\,||F_o|-|F_c||/\Sigma\,|F_o|$ for the 1469 measured data was initially 0·36. Convergence was rapid and led to $R=0{\cdot}038$. The structure model (see *Description of the structure*) suggested that the somewhat higher-than-normal isotropic temperature factors for Mg(1) and Mg(2) might be due to an anisotropic motion of high amplitude in the hexagonal **c** direction. This assumption was confirmed after a few additional refinement cycles in which anisotropic thermal parameters were included for each atom in the then 81×81 full matrix. In the course of this refinement, empirical correction factors for secondary extinction (Zachariasen, 1963) were applied to the 92 strongest reflections. The R index decreased to 0·021. The final goodness of fit $\Sigma\,\omega(F_o^2-F_c^2)^2/(m-S)$ is 1·36. The positional parameters obtained from this anisotropic refinement differed insignificantly from those obtained with the isotropic treatment.

After having taken notice of our brief report on the completed work (Samson & Gordon, 1966), Professor David Shoemaker very kindly brought to our attention the possibility that ε-$Mg_{23}Al_{30}$ might be isostructural with the R(Mo–Co–Cr) phase (Komura, Sly & Shoemaker, 1960), which crystallizes also with a rhombohedral unit cell ($a_0=9{\cdot}011$ Å, $\alpha=74°27{\cdot}5'$) that contains 53 atoms arranged according to space group $R\bar{3}$. To facilitate comparison of the structural parameters of the two phases, we have included in Table 2 the atom-identification symbols used for the R phase. It can be seen that two coordinates [for Mg(2) and Al(11)] differ by about 0·5 Å and nine by 0·1 to 0·3 Å from the corresponding ones in the R phase. Accordingly, not all parts of the structural motifs are the same in the two phases; the differences will be described in the following sections.

For direct comparison of our parameters with those of the R phase, x and y have to be interchanged and z has to be replaced by $1-z$.

Description of the structure

The dominant part of the structure consists of an infinite, three-dimensional framework of Friauf polyhedra that are arranged along the edges of the rhombohedral unit cells; one such cell is shown in Fig. 1(*c*). The Friauf polyhedra are, in the crystallographic sense, of two different kinds; the dark ones are called $F1$ [around Mg(3)], and the light ones are called $F2$ [around Mg(4)]. The origin of each rhombohedral cell coincides with the center of a hexagon that is shared between two Friauf polyhedra of the dark kind ($F1$).

Each dark polyhedron ($F1$) shares three of its four hexagons with three light polyhedra ($F2$) and one hexagon with a dark polyhedron ($F1$), as is shown in Fig. 1(*a*). Each light polyhedron ($F2$) shares one hexagon with another light polyhedron ($F2$) and one with a dark polyhedron ($F1$), as shown in Fig. 1(*b*). The atom out from the center of the third hexagon of $F2$ (light) constitutes a vertex of a truncated tetrahedron of an adjacent $F2$-polyhedron; two such vertices are marked out in Fig. 1(*b*) and shall be referred to later as the 'hybrid' vertices. The coordination shell around each such vertex [Mg(6)] is a hexagonal antiprism that has two atoms at the extended poles (ligancy 14). The fourth hexagon of $F2$ is shared with another such $L14$ shell (L=ligancy), which has Mg(5) at its center.

The arrangement of polyhedra along the [111] direction (threefold axis) of the rhombohedron is most conveniently described by starting out with the highly idealized form as it occurs in the R phase (see preceding section); this is shown in Fig. 1(*d*). The sequence of polyhedra is: (1) the dark Friauf polyhedron $F1$; (2) three centered icosahedra (*a*), (*b*), and (*c*), sharing triangles with one another and $F1$; (3) again a Friauf polyhedron of the dark kind $F1$. In ε-$Mg_{23}Al_{30}$ the polyhedra (1) and (3) are unchanged, but the central icosahedron (*b*) is replaced by a coordination shell of ligancy 14, and (*a*) and (*c*) each by a coordination shell of ligancy 13, as is shown in the stereo picture Fig. 2. It can be seen that these three shells are arrived at by widening the central icosahedron (*b*) perpendicular to [111] so that the atom Mg(1) at its center comes in contact with the two atoms of the kind Mg(2) at the centers of (*a*) and (*c*). The coordination shell around Mg(1) (center of rhombohedron) can be made out as a distorted hexagonal prism that has two atoms at the extended poles, and the center of each prism face represents an octahedral interstice and not a tetrahedral one that is observed at this place in the R phase. This coordination shell is shown separately in Fig. 3.

It is seen (Fig. 2) that the three coordination shells ($L13$, $L14$, $L13$) form a channel around [111] and that the atoms Mg(1) and Mg(2) undergo anisotropic motions of somewhat higher amplitude in the direction of the channel as was pointed out under *Refinement*. The channel (Fig. 2) comprises all the 11 crystallographically different atoms.

The coordination shells around Al(7), Al(8), Al(9), and Al(10) are icosahedra. Al(11) is surrounded by a shell of ligancy 11, which may be described as an icosahedron (pentagonal antiprism with two atoms at the extended poles) in which one pentagon has been replaced by a tetragon.

Discussion of the coordination polyhedra

The unit rhombohedron contains eight Friauf polyhedra [around Mg(3) and Mg(4)], 24 centered icosahedra [around Al(7), Al(8), Al(9), and Al(10)], 13 centered polyhedra of ligancy 14 [around Mg(1), Mg(5), and Mg(6)], two centered polyhedra of ligancy 13 [around Mg(2)], and six centered polyhedra of ligancy 11 [around Al(11)], all of which have been described in the preceding section.

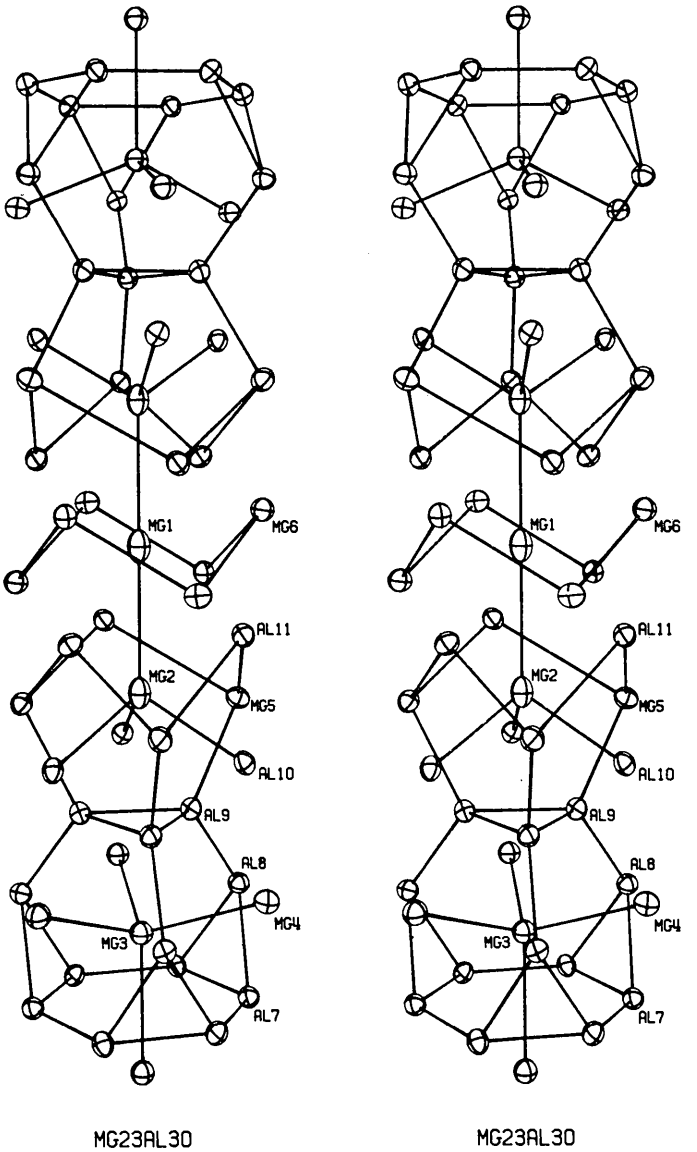

Fig. 2. A stereoscopic representation of the polyhedra along the threefold axis in ε-$Mg_{23}Al_{30}$. It is seen that Mg(1) and Mg(2) perform anisotropic motions of increased amplitude in the direction of the channel formed by the polyhedra.

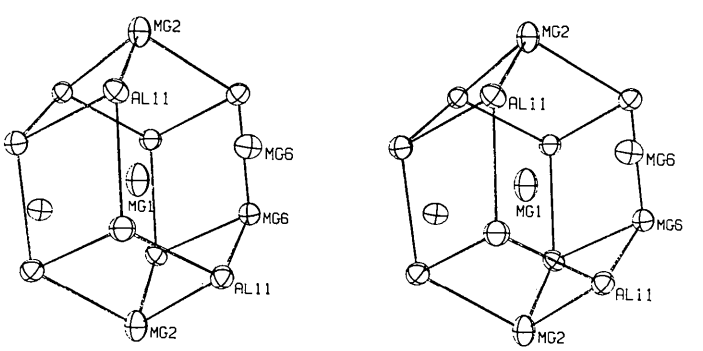

Fig. 3. A stereoscopic representation of the $L14$ shell around Mg(1), the hexagonal prism with two atoms at the extended poles.

Each of the 12 vertices of the truncated tetrahedron of $F1$ [6 Al(7)+3 Al(8)+3 Al(9)] represents the center of an icosahedron, while each truncated tetrahedron of $F2$ is penetrated by ten icosahedra [2 Al(7)+3 Al(8) +3 Al(9)+2 Al(10)], one coordination shell of ligancy 14 [hybrid vertex, Mg(6)], and one of ligancy 11 [Al(11)]. Hence, each corner of a facet in Fig. 1(*c*) represents the center of an icosahedron, with the exception of 24 corners that represent centers of $L11$ shells [Al(11)] and 24 that represent centers of $L14$ shells [Mg(6)]. In fact, Fig. 1(*c*) may be regarded as representing a set of 240 points, of which 192 are icosahedron centers. The basic building block thus appears to be the icosahedron, and the Friauf-polyhedra framework may be regarded as describing mainly the modes in which the icosahedra interpenetrate.

Some metrical data on these polyhedra are given in Tables 6 to 9. Comparison of these tables with those given for β-Mg_2Al_3 (Samson, 1965) and Cu_4Cd_3 (Samson, 1967*a*) reveals the existence of striking metrical similarities. Of the 34 crystallographically different icosahedra observed in the three structures, 30 have a D/E ratio which is somewhat smaller than that corresponding to a regular icosahedron, and in each case about half the vertices are occupied by large atoms (here magnesium) and the other half by small atoms (here aluminum).

A detailed description of a variety of features that are prevalent in structures incorporating Friauf polyhedra and icosahedra has been given recently (Samson, 1967*a*,*b*, 1968).

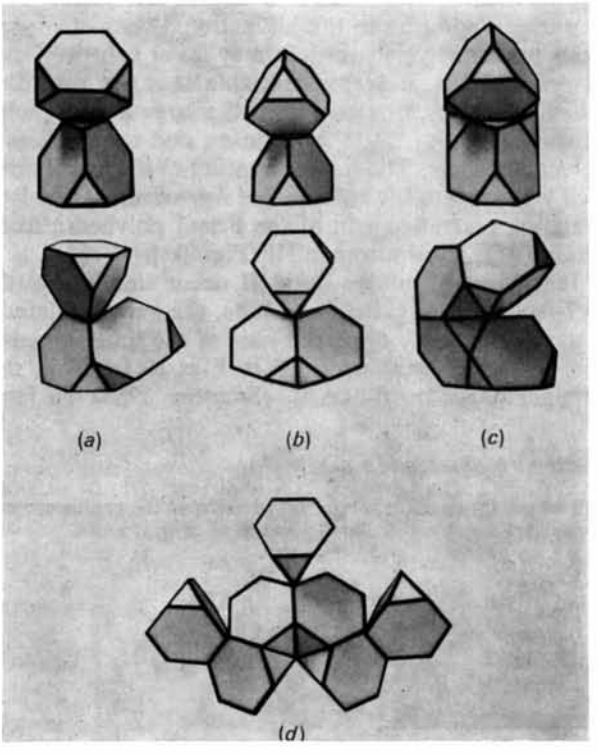

Fig. 4. The three modes in which Friauf polyhedra create bifunctional or hybrid vertices and give rise to misfit. They are often observed in conjunction with substitutional and displacement disorder. DA = dihedral angle between the hexagon and the triangle, AA = distance between hybrid vertex and center of adjacent Friauf polyhedron, PD = distortion of triangle; see text. (*a*) Mode I. $DA = 31°36'$, $AA = 1{\cdot}07a$, $PD = 1{\cdot}17a$; in γ-$Mg_{17}Al_{12}$, χ phases, and β-Mg_2Al_3. (*b*) Mode II. $DA = 35°16'$, $AA = 1{\cdot}12a$, $PD = 1{\cdot}22a$; in β-Mg_2Al_3 only. (*c*) Mode III. $DA = 38°56'$, $AA = 1{\cdot}17a$, $PD = 1{\cdot}29a$; in ε-$Mg_{23}Al_{30}$ and R phases. (*d*) Mixture of modes I and II, as observed in β-Mg_2Al_3.

Table 5. *Interatomic distances and bond numbers*

The calculated valences are listed in Tables 6, 8, and 9. The number in parentheses following the name of a polyhedron is the identification number referred to as ID.

Kind of Atom	Ligancy	Distance Å	Bond No. n
Mg(1)	2 Mg(2)	3.496	0.052
	6 Mg(6)	3.120	0.223
	6 Al (11)	3.263	0.082
	14, hexagonal prism +2 (1)		
Mg(2)	1 Mg(1)	3.496	0.052
	3 Mg(5)	3.199	0.164
	3 Al (9)	3.397	0.049
	3 Al (10)	3.012	0.216
	3 Al (11)	2.889	0.345
	13, polyhedron (3)		
Mg(3)	3 Al (7)	3.118	0.144
	3 Al (7)	3.158	0.123
	3 Al (8)	3.256	0.084
	3 Al (9)	3.141	0.131
	1 Mg(3)	3.354	0.091
	3 Mg(4)	3.298	0.112
	16, Friauf polyhedron F1		
Mg(4)	1 Mg(6)	3.148	0.200
	1 Al (7)	3.115	0.145
	1 Al (7)	3.148	0.128
	1 Al (8)	3.082	0.165
	1 Al (8)	3.115	0.145
	1 Al (8)	3.278	0.078
	1 Al (9)	3.125	0.140
	1 Al (9)	3.205	0.103
	1 Al (9)	3.245	0.088
	1 Al (10)	3.238	0.090
	1 Al (10)	3.260	0.083
	1 Al (11)	3.125	0.140
	1 Mg(3)	3.298	0.112
	1 Mg(4)	3.303	0.110
	1 Mg(5)	3.147	0.200
	1 Mg(6)	3.818	0.015
	16, Friauf polyhedron F2		
Mg(5)	1 Mg(2)	3.199	0.164
	1 Mg(4)	3.147	0.200
	1 Mg(5)	3.105	0.236
	1 Mg(6)	3.232	0.144
	1 Mg(6)	3.269	0.126
	1 Al (7)	3.177	0.114
	1 Al (7)	3.231	0.093
	1 Al (8)	3.284	0.076
	1 Al (9)	2.970	0.244
	1 Al (10)	2.968	0.255
	1 Al (10)	3.037	0.196
	1 Al (10)	3.166	0.119
	1 Al (11)	3.010	0.217
	1 Al (11)	3.165	0.120
	14, hexagonal antiprism +2 (5)		
Mg(6)	1 Mg(1)	3.120	0.223
	1 Mg(4)	3.148	0.200
	1 Mg(4)	3.818	0.015
	1 Mg(5)	3.232	0.145
	1 Mg(5)	3.269	0.126
	1 Mg(6)	3.471	0.058
	1 Mg(6)	3.471	0.058
	1 Al (8)	2.988	0.237
	1 Al (8)	3.092	0.158
	1 Al (9)	3.113	0.146
	1 Al (10)	3.030	0.201
	1 Al (11)	2.835	0.425
	1 Al (11)	3.004	0.222
	1 Al (11)	3.228	0.094
	14, hexagonal antiprism +2 (6)		
Al(7)	1 Mg(3)	3.118	0.144
	1 Mg(3)	3.158	0.123
	1 Mg(4)	3.115	0.145
	1 Mg(4)	3.148	0.128
	1 Mg(5)	3.177	0.114
	1 Mg(5)	3.231	0.093
	2 Al (7)	2.653	0.549
	1 Al (8)	2.781	0.335
	1 Al (8)	2.786	0.328
	1 Al (10)	2.791	0.323
	1 Al (11)	2.762	0.360
	12, icosahedron (7)		
Al(8)	1 Mg(3)	3.256	0.084
	1 Mg(4)	3.082	0.165
	1 Mg(4)	3.115	0.145
	1 Mg(4)	3.278	0.078
	1 Mg(5)	3.284	0.076
	1 Mg(6)	2.988	0.237
	1 Mg(6)	3.092	0.159
	1 Al (7)	2.781	0.335
	1 Al (7)	2.786	0.328
	1 Al (9)	2.648	0.559
	1 Al (10)	2.755	0.371
	1 Al (11)	2.732	0.405
	12, icosahedron (8)		
Al(9)	1 Mg(3)	3.141	0.131
	1 Mg(2)	3.397	0.049
	1 Mg(4)	3.125	0.140
	1 Mg(4)	3.205	0.103
	1 Mg(4)	3.245	0.088
	1 Mg(5)	2.980	0.244
	1 Mg(6)	3.113	0.146
	1 Al (8)	2.648	0.559
	2 Al (9)	2.769	0.350
	1 Al (10)	2.726	0.414
	1 Al (10)	2.791	0.323
	12, icosahedron (9)		
Al(10)	1 Mg(2)	3.012	0.216
	1 Mg(4)	3.238	0.090
	1 Mg(4)	3.260	0.083
	1 Mg(5)	2.968	0.255
	1 Mg(5)	3.037	0.196
	1 Mg(5)	3.166	0.119
	1 Mg(6)	3.030	0.201
	1 Al (7)	2.791	0.322
	1 Al (8)	2.755	0.371
	1 Al (9)	2.726	0.414
	1 Al (9)	2.791	0.323
	1 Al (11)	2.933	0.187
	12, icosahedron (10)		
Al(11)	1 Mg(1)	3.263	0.082
	1 Mg(2)	2.889	0.345
	1 Mg(4)	3.125	0.140
	1 Mg(5)	3.010	0.217
	1 Mg(5)	3.165	0.120
	1 Mg(6)	2.835	0.425
	1 Mg(6)	3.004	0.222
	1 Mg(6)	3.228	0.094
	1 Al (7)	2.762	0.360
	1 Al (8)	2.732	0.405
	1 Al (10)	2.933	0.187
	11, polyhedron (11)		

General discussion of the structure

It is now seen that each of the three intermetallic compounds in the magnesium–aluminum system, γ-$Mg_{17}Al_{12}$, β-Mg_2Al_3, and ε-$Mg_{23}Al_{30}$, is built up of a complex, three-dimensional framework of Friauf polyhedra that are penetrated by icosahedra.

The structure of the χ phases (Kasper, 1954, Greenfield & Beck, 1956) corresponds to that of γ-$Mg_{17}Al_{12}$ (variable composition), but the *R*-phase structure (Komura, Sly & Shoemaker, 1960) has only some of its structural features in common with ε-$Mg_{23}Al_{30}$. Whereas the ε structure incorporates eight Friauf polyhedra, 24 icosahedra, 13 polyhedra of *L*14, two of *L*13, and six of *L*11, the *R*-phase structure has eight Friauf polyhedra, 27 icosahedra, 12 polyhedra of *L*14, and six of *L*15. It does not seem justified, therefore, to call *R* and ε fully isostructural but rather homotypical (closely related structures).

Misfit of polyhedra (manifestation of disorder)

An interesting feature is the occurrence of 'hybrid' vertices in each of the structures just discussed; see also Fig. 4. This is a vertex of a truncated tetrahedron [at which a small atom (here, aluminum) normally is expected] that represents simultaneously the atom out from the center of a hexagon of an adjacent truncated tetrahedron, which normally is of the large kind (here, magnesium). This vertex, accordingly, fills two disparate functions. The coordination shell around it is sometimes of the intermediate ligancy 14 (β-Mg_2Al_3, ε-$Mg_{23}Al_{30}$, and *R* phases) and sometimes of ligancy 13 (γ-$Mg_{17}Al_{12}$ and χ phases), depending upon the mode in which the hybrid vertex is created. Mode I [Fig. 4(*a*)] is observed in γ-$Mg_{17}Al_{12}$ and the χ phases, mode II [Fig. 4(*b*)] in β-Mg_2Al_3, and mode III [Fig. 4(*c*)] in ε-$Mg_{23}Al_{30}$ and the *R* phases.

If each truncated tetrahedron were regular and each of its 18 edges were of length *a*, then the dihedral angle between the hexagon and the equilateral triangle shown in Fig. 4(*a*) (mode I) would be 31°36′, in Fig. 4(*b*) (mode II) 35°16′, and in Fig. 4(*c*) (mode III) 38°56′. In each case the hybrid vertex lies below the normal that passes through the center of the hexagon. In order that this vertex be equidistant from all six corners of the hexagon (with the dihedral angles unchanged) the equilateral triangle has to be converted into an isosceles triangle in which the two shanks are of length 1·17*a* (mode I), 1·22*a* (mode II), or 1·29*a* (mode III), which involves a significant distortion. The distance between the hybrid vertex and the center of the adjacent Friauf polyhedron (*A*–*A* distance) is 1·07*a* for mode I, 1·12*a* for mode II, and 1·17*a* for mode III, whereas the center-to-center distance between two truncated tetrahedra that share a hexagon is 1·23*a*.

It is seen that at least one of the Friauf polyhedra must be significantly distorted, although all the truncated tetrahedra may be regular, as is the case in Fig. 4. The creation of the hybrid vertices, accordingly, is associated with a considerable degree of misfit. This feature, in addition to the bifunctional character, suggests that the hybrid vertices may favor substitutional disorder. Thus, it seems probable that the disorder, which must be associated with the large homogeneity ranges of γ-$Mg_{17}Al_{12}$, the χ phases, and the *R* phases, is localized here. The transformation of the aluminum-rich γ phase into the ε phase (see *Introduction*) involves mainly a rearrangement of the Friauf polyhedra from mode I [Fig. 4(*a*)] to mode III [Fig. 4(*c*)].

In β-Mg_2Al_3, modes I and II occur simultaneously as is shown in Fig. 4(*d*), and here, the vertex of mode I was found to be displaced part of the time; see also the polygonal section of *F*3 in Figs. 10 to 17 in the original paper on β-Mg_2Al_3 (Samson, 1965). In fact,

Table 6. *Some metrical data on the icosahedra observed in* ε-$Mg_{23}Al_{30}$

N = number of icosahedra per unit rhombohedron, *E* = average length of the thirty edges, *D* = average value of the twelve center-to-vertex distances, Mg, Al = number of respective atom at the vertices, *V* = calculated valence of central atom.

Central atom	*N*	*E*	*D*	*D*/*E*	Mg	Al	*V*
Al(7)	6	3·116	2·948	0·946	6	6	3·19
Al(8)	6	3·152	2·983	0·946	7	5	2·94
Al(9)	6	3·167	2·992	0·945	7	5	2·90
Al(10)	6	3·145	2·975	0·946	7	5	2·78
	24						

Table 7. *Metrical data and dihedral angles of the truncated tetrahedra observed in* ε-$Mg_{23}Al_{30}$

ID = identification number (see Table 5). *N*, *E*, *D*, and *D*/*E* have similar meanings to those in Table 6. There are 18 edges (*E*) and 12 center-to-vertex distances (*D*). The dihedral angles given in columns 7 and 8 are those between the hexagons (least-squares planes).

ID	Central atom	*N*	*E*	*D*	*D*/*E*	Dihedral angles		Mg	Al
*F*1	Mg(3)	2	2·715	3·168	1·167	69·9°	71·2°	0	12
*F*2	Mg(4)	6	2·778	3·229	1·162	68·2	72·8	1	11
		8							

all the disorder observed in β-Mg_2Al_3 is confined to the regions containing hybrid vertices.

VEC *rule and interatomic distances*

An interesting contrast between the two magnesium–aluminum phases γ and ε and their homotypes in the transition-metal systems is the general trend in the 'valence-electron concentration' (VEC). Das & Beck (1960) pointed out that in the sequence σ, P, R, μ, α-Mn (α-Mn is isostructural with γ-$Mg_{17}Al_{12}$) 'the VEC increases and that this provides a qualitative support to the interpretation of these phases as electron compounds'. It is seen that in the magnesium–aluminum system this trend is reversed, since ε-$Mg_{23}Al_{30}$ has a VEC of $2{\cdot}57 \pm 0{\cdot}02$, and the γ phase, which exists over a range extending from approximately $Mg_{13}Al_{16}$ (VEC=2·55) to $Mg_{17}Al_{12}$ (VEC=2·41) at 450°C, exhibits at room temperature an increasing stability as the VEC *decreases* (refer also to the *Introduction* at the beginning of this paper). We should like to emphasize at this point that we have invested considerable effort and time in the experimental work in order to establish confidence in the correctness of our VEC treatment; detailed structure studies of spherically ground single crystals of various compositions of the γ-(Mg,Al) phase are under way.

Table 8. *Metrical data on the Friauf polyhedra*

All column headings have similar meanings to those in Table 7. V=calculated valence of central atom. There are 48 edges (E) and 16 center-to-vertex distances (D).

ID	E	D	D/E	Mg	Al	V
$F1$	2·971	3·204	1·078	4	12	1·87
$F2$	2·992	3·228	1·079	5	11	1·94

Table 9. *Data on miscellaneous kinds of polyhedra*

The column headings have a similar meaning to those in Tables 6 and 7. L=ligancy of central atom.

Central atom	N	L	Mg	Al	V
Al(11)	6	11	8	3	2·60
Mg(2)	2	13	4	9	2·37
Mg(1)	1	14	8	6	1·93
Mg(5)	6	14	5	9	2·30
Mg(6)	6	14	7	7	2·31
	21				

The interatomic distances (Table 5) as well as the metallic valences (Tables 6,8,9), calculated according to the formula $D_n = D_1 - 0{\cdot}600 \log_{10} n$ (Pauling, 1947), show the same kind of spread as in β-Mg_2Al_3. The shortest Al–Al distance is here 2·65 Å as compared with 2·56 Å observed in β-Mg_2Al_3, 2·69 Å in $Mg_3Cr_2Al_{18}$ (Samson, 1958), and 2·66 Å in $Mg_2Cu_6Al_5$ (Samson, 1949).

We thank Mr K. Christiansson and Mrs B. Christiansson for their success in preparing the single crystals and Professor David P. Shoemaker for directing our attention to the R-phase structure.

References

BERGMAN, G. B., WAUGH, L. T. & PAULING, L. (1957). *Acta Cryst.* **10**, 254.
BOND, W. L. (1951). *Rev. Sci. Instrum.* **22**, 344.
BURBANK, R. D. (1965). *Acta Cryst.* **19**, 957.
CLARK, J. B. & RHINES, F. N. (1957). *J. Metals*, **9**, 6.
DAS, B. N. & BECK, P. A. (1960). *AIME, Trans.* **218**, 733.
DUCHAMP, D. J. (1964). Amer. Cryst. Assoc. Meeting, Bozeman, Montana, paper B-14, p.29.
EICKHOFF, K. & VOSSKÜHLER, H. (1953). *Z. Metallk.* **44**, 223.
GREENFIELD, P. & BECK, P. A. (1956). *J. Metals*, **8**, 265.
International Tables for X-ray Crystallography (1952). Vol.I. Birmingham: Kynoch Press.
International Tables for X-ray Crystallography (1962). Vol.III. Birmingham: Kynoch Press.
KASPER, J. S. (1954). *Acta Metallurg.* **2**, 456.
KOMURA, Y., SLY, W. G. & SHOEMAKER, D. P. (1960). *Acta Cryst.* **13**, 575.
KURNAKOV, N. S. & MIKHEEVA, V. I. (1938). *Izvest. Sekt. Fiziko-Khim. Anal.* **10**, 5.
LAVES, F., LÖHBERG, K. & RAHLFS, P. (1934). *Nachr. Ges. Wiss. Göttingen* Fachgr. IV, **1**, 67.
PAULING, L. (1947). *J. Amer. Chem. Soc.* **69**, 542.
PEPINSKY, R. & JARMOTZ, P. (1948). *Rev. Sci. Instrum.* **19**, 247.
PERLITZ, H. (1944). *Nature, Lond.* **154**, 607.
PERLITZ, H. (1946). *Chalmers Tekniska Högskolans Handlingar*, **50**, 1.
PETERSON, S. W. & LEVY, H. A. (1957). *Acta Cryst.* **10**, 70.
RENNINGER, M. (1937). *Z. Physik*, **106**. 141.
SAMSON, S. (1949). *Acta Chem. Scand.* **3**, 809.
SAMSON, S. (1958). *Acta Cryst.* **11**, 851.
SAMSON, S. (1964). *Acta Cryst.* **17**, 491.
SAMSON, S. (1965). *Acta Cryst.* **19**, 401.
SAMSON, S. (1966). *Rev. Sci. Instrum.* **37**, 1255.
SAMSON, S. & GORDON, E. K. (1966). Annual Report: Chemistry and Chemical Engineering, California Institute of Technology p .34.
SAMSON, S. (1967*a*). *Acta Cryst.* **23**, 586.
SAMSON, S. (1967*b*). *Structural Chemistry and Molecular Biology*. San Francisco: W.H. Freeman. In the press.
SAMSON, S. (1968). *Structural Developments in Alloy Phases*. New York: Gordon and Breach. In the press.
SAMSON, S. & SCHUELKE, W. (1967). *Rev. Sci. Instrum.* **38**, 1273.
SHORT, M. A. (1960). *Rev. Sci. Instrum.* **31**, 618.
ZACHARIASEN, W. H. (1963). *Acta Cryst.* **16**, 1139.